INTERFACE

Research

Author for correspondence:
Martin Schuster
e-mail: martin.schuster@oregonstate.edu

THE ROYAL SOCIETY
PUBLISHING

Parameters, architecture and emergent properties of the *Pseudomonas aeruginosa* LasI/LasR quorum-sensing circuit

Martin Schuster[1], Christina Li[1], Parker Smith[1] and Christina Kuttler[2]

[1]Department of Microbiology, Oregon State University, Corvallis, OR 97331, USA
[2]Department of Mathematics, Technische Universität München, 85748 Garching, Germany

(iD) MS, 0000-0002-7674-0887; CK, 0000-0002-5521-4159

Quorum sensing is a widespread process in bacteria that controls collective behaviours in response to cell density. Populations of cells coordinate gene expression through the perception of self-produced chemical signals. Although this process is well-characterized genetically and biochemically, quantitative information about network properties, including induction dynamics and steady-state behaviour, is scarce. Here we integrate experiments with mathematical modelling to quantitatively analyse the LasI/LasR quorum sensing pathway in the opportunistic pathogen *Pseudomonas aeruginosa*. We determine key kinetic parameters of the pathway and, using the parametrized model, show that quorum sensing behaves as a bistable hysteretic switch, with stable on and off states. We investigate the significance of feedback architecture and find that positive feedback on signal production is critical for induction dynamics and bistability, whereas positive feedback on receptor expression and negative feedback on signal production play a minor role. Taken together, our data-based modelling approach reveals fundamental and emergent properties of a bacterial quorum sensing circuit, and provides evidence that native quorum sensing can indeed function as the gene expression switch it is commonly perceived to be.

1. Introduction

Cell–cell communication, termed quorum sensing (QS), is a common process in bacteria that regulates collective behaviours according to population cell density by producing and sensing diffusible autoinducer (AI) molecules [1,2]. QS-controlled behaviours range from interactions with eukaryotic hosts and microbial warfare to protein secretion and biofilm formation. In Gram-negative bacteria, the basic QS circuitry consists of a LuxI-type synthase that produces an acyl-homoserine lactone (AHL) signal, and a cognate LuxR-type signal receptor [3,4]. The diffusible AHL signal accumulates during growth, binds to the LuxR-type receptor and activates the expression of target genes, as well as the expression of the synthase itself.

QS has been extensively characterized genetically and biochemically, revealing important information about the function and regulation of individual components, target genes, induction kinetics, and signal specificity [4–6]. QS via AHL is particularly well understood in the Gram-negative model organism and opportunistic human pathogen *Pseudomonas aeruginosa* [5,6]. In *P. aeruginosa*, QS controls hundreds of genes, including extracellular enzymes, toxins, metabolites and biofilm components [7–9]. The major AHL system (termed '*las*') consists of the LuxI-type synthase LasI that produces 3-oxo-dodecanoyl-homoserine lactone (3OC12-HSL) and the LuxR-type intracellular receptor LasR that binds the signal and dimerizes to activate transcription of target genes (figure 1). One of these target genes is *lasI*, creating a positive feedback loop [10]. For *lasR*, evidence of positive feedback-control is less clear [7,11,12]. In addition, the transcription of *lasI* is subject to negative regulation by the repressor RsaL, which is itself induced by LasR-3OC12-HSL, dampening
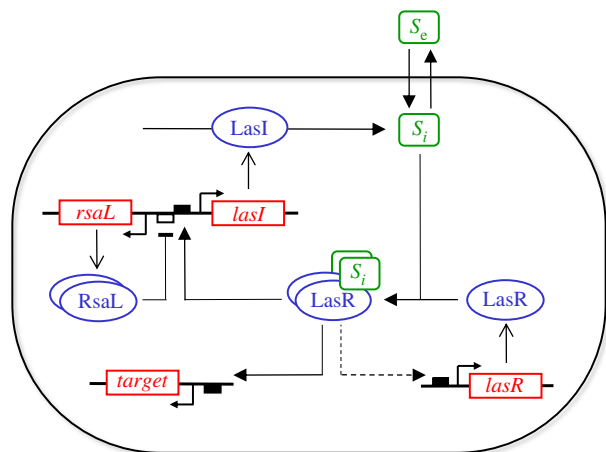
Figure 1. *Pseudomonas aeruginosa las* QS circuit. Red symbols indicate genes, blue symbols indicate proteins, and green symbols indicate small molecules. S_e and S_i denote extracellular and intracellular 3OC12-HSL signal, respectively; *target* represents one of many target genes in the LasR regulon. Shown are signal exchange, receptor dimerization upon signal binding, positive feedback on *lasI* and *lasR*, as well as negative feedback on *lasI* and *rsaL*. Black boxes indicate LasR binding sites, and the open box in the *lasI-rsaL* bidirectional promoter indicates an RsaL binding site.

signal accumulation during culture growth [13,14]. Movement of 3OC12-HSL across the cell envelope is probably by a combination of diffusion and active transport [15,16]. In this study, we will focus our analysis on the *las* QS system, acknowledging that there are other, subordinate QS systems (*rhl*, *PQS*) in *P. aeruginosa* [6].

As described, the *P. aeruginosa las* system enables coordinated gene expression control at the population level, where the accumulation of extracellular 3OC12-HSL produced by all cells triggers a concerted response [17,18]. This behaviour is consistent with the general perception of QS as a population switch [19–21], although some systems also exhibit heterogeneous responses with considerable cell-to-cell variation [22–26].

In addition to experimental inquiry, QS has been investigated from a theoretical perspective. Mechanistic mathematical modelling studies have revealed important insights into architecture and emergent properties of the signalling network [27–36]. Theory predicts that the *P. aeruginosa las* QS system, with positive feedback and receptor dimerization as two key elements, may constitute a bistable system with two stable states, on and off [30]. Bistability has been considered a hallmark of the canonical QS circuitry, yet it has rarely been demonstrated experimentally [27–29]. The only two cases we are aware of employ a non-native heterologous host system [26,37]. An important accompanying property of bistability is hysteresis, the dependency of the steady-state response on the direction of the parameter change. Hysteresis has functional implications by increasing the robustness of the QS response to fluctuations in environmental signal levels [26].

In this study, we have combined experimental and theoretical approaches for a data-centred analysis of the *P. aeruginosa las* QS system. We collected extensive experimental data, built a mechanistic mathematical model, and fit the model to the data. Using the parametrized model, we investigated emergent properties including bistability and hysteresis, as well as the role of positive and negative feedback. Our findings help define the design principles and functional capacity of QS systems.

2. Methods

2.1. Bacterial strains, plasmids and growth conditions

We used the *P. aeruginosa* PAO1 wild-type strain (WT, Iglewski lineage) [38], and an isogenic mutant containing a markerless in-frame deletion in *lasI* [18]. We used the promoter-probe vector pPROBE.AT [39] with *lasI'-gfp*, *lasR'-gfp* and *rsaL'-gfp* transcriptional fusions, respectively. The encoded green fluorescent protein (GFP) variant is the stable and fast-folding *gfpmut1* [40]. The *lasI'-gfp* and *rsaL'-gfp* fusion constructs were described previously [18], whereas the *lasR'-gfp* fusion was constructed for the present study, using routine molecular cloning techniques. A 333 bp *lasR* promoter region was PCR-amplified from the PAO1 genome using forward primer 5'-N6AAGCTTGCGATGGGCC GACAGTGAAC-3' and reverse primer 5'-N6GAATTCTCTTAAA CTATTAACCAATCAGCCAAATATGGATT-3'. The PCR product was digested with *Hin*dIII and *Eco*RI (restriction sites underlined) and ligated with equally digested pProbe-AT. The resulting construct was confirmed by sequencing. Plasmids were introduced into chemically competent *P. aeruginosa* strains according to standard procedures [41]. Strains were grown at 37°C with shaking in Lennox Lysogeny Broth (LB) liquid cultures buffered with 50 mM 3-(*N*-morpholino)-propanesulfonic acid (MOPS), pH 7.0, or on LB agar plates. The antibiotic carbenicillin was added at a final concentration of 200 μg ml^{-1} for plasmid selection and maintenance. Growth was measured as optical density at 600 nm (OD_{600}) in a photometer (Eppendorf Biophotometer), and as colony-forming units (CFU) per ml by dilution-plating. The conversion factor between OD_{600} and CFU ml^{-1} was determined by linear regression (electronic supplementary material, figure S1).

2.2. Gene expression and AHL measurements

We conducted gene expression and AHL quantitation of *P. aeruginosa* strains in LB-MOPS liquid cultures. We employed a pre-culturing scheme as described previously to dilute pre-existing GFP in cells to background levels [18]. In short, we inoculated pre-cultures with freshly streaked *P. aeruginosa* colonies, and grew them to an OD_{600} of 0.1 to 0.2. Using these pre-cultures, we inoculated experimental cultures to an initial OD_{600} of 0.001. Cultures were grown for 3 h before the first sampling. Subsequent samples were taken every 0.5 to 1 h, for up to 12h of total cultivation time. For gene expression analysis, *P. aeruginosa* WT and *lasI* mutant strains contained *lasI'-gfp*, *lasR'-gfp* or *rsaL'-gfp* reporter fusions. At each time point, aliquots were transferred to a black-walled microtiter plate to quantify GFP intensity in a fluorescence plate reader (Tecan M200) at 480 nm excitation and 535 nm emission wavelengths. The fluorescence of LB-MOPS medium was subtracted as a blank. The net fluorescence values were divided by the OD_{600} at the respective time point to attain relative fluorescence intensities.

For AHL analysis, at each time point a 5 ml culture aliquot was extracted twice with acidified ethyl acetate as described in [42,43]. Extracts were concentrated to dryness by evaporation and resuspended in fresh ethyl acetate. The 3OC12-HSL content in these extracts was determined by an established *Escherichia coli* bioassay containing *lasR* and a *lasB'-lacZ* reporter [42,43]. ß-galactosidase activity of bioassay cultures was measured using the Galacto Light Plus Reporter Gene Assay (Thermo Fisher). 3OC12-HSL concentrations in the experimental samples were determined by comparison with a standard curve generated with synthetic 3OC12-HSL (RTI International).

2.3. Mathematical model

Mathematical modelling was based on a previously described quantitative model of QS [28,44]. This model consists of a system of ordinary differential equations (ODEs) that describes

the change in signal and protein components, as well as cell growth, over time. Parameters are described in table 1. We considered the cellular signalling dynamics with two different versions of this model: (i) a minimal model with positive feedback on *lasI* expression only, and (ii) an extended model with positive feedback on both *lasI* and *lasR* expression, as well as negative feedback on *lasI* and *rsaL* expression via RsaL. The minimal model is described as follows:

extracellular 3OC12-HSL, S_e

$$\frac{dS_e}{dt} = \rho_v\, c_{sec}\, (S_i - S_e) - \gamma_{ex}\, S_e,$$

intracellular 3OC12-HSL, S_i

$$\frac{dS_i}{dt} = c_{sec}\, (S_e - S_i) + A_{syn}\, I$$

and LasI synthase, I

$$\frac{dI}{dt} = (V_{I\,max} - V_{I\,min})\, \frac{S_i^{\,m}}{S_i^{\,m} + K_S^m} + V_{I\,min} - \gamma_I\, I.$$

The minimal model is virtually identical to that by Fujimoto and Sawai [28]. It makes several assumptions and simplifications. It models the positive feedback of 3OC12-HSL on *lasI* expression directly through the Hill function $S_i^m/(S_i^m + K_S^m)$ and does not explicitly model LasR. However, it considers positive cooperativity (expressed by the Hill coefficient m), which primarily manifests through receptor dimerization [49]. The binding of one signal molecule to a receptor monomer, which then drives dimerization, is assumed to be non-cooperative, as is the binding of LasR-3OC12-HSL to target promoters [53,54]. The model omits the concentrations of mRNA species, as they are assumed to be in quasi-steady state with the respective protein concentrations [27]. It considers extracellular but not intracellular signal degradation, because the contribution of intracellular degradation is negligible, given the extremely small intracellular volume fraction. The model also does not distinguish between contributions of diffusion and active transport to the movement of signal in and out of the cell [16], and does not explicitly consider potential effects of growth rate on the concentrations of intracellular species [55]. These simplifications reduce the complexity of the model such that parameter estimation is computationally feasible. The cellular volume fraction (ρ_v) affects the extracellular 3OC12-HSL concentration (S_e) through population growth, as described below.

In addition to the minimal model, we built the following extended model that incorporates additional protein components and feedback regulation:

extracellular 3OC12-HSL, S_e

$$\frac{dS_e}{dt} = \rho_v\, c_{sec}\, (S_i - S_e) - \gamma_{ex}\, S_e,$$

intracellular 3OC12-HSL, S_i

$$\frac{dS_i}{dt} = c_{sec}\, (S_e - S_i) + A_{syn}\, I,$$

LasI synthase, I

$$\frac{dI}{dt} = (V_{I\,max} - V_{I\,min})\, \frac{(RS_i)^m}{(RS_i)^m + K_S^m}\, \frac{K_{L1}^n}{L^n + K_{L1}^n} + V_{I\,min} - \gamma_I\, I,$$

LasR receptor, R

$$\frac{dR}{dt} = (V_{R\,max} - V_{R\,min})\, \frac{(RS_i)^m}{(RS_i)^m + K_S^m} + V_{R\,min} - \gamma_R\, R$$

and RsaL repressor, L

$$\frac{dL}{dt} = (V_{L\,max} - V_{L\,min})\, \frac{(RS_i)^m}{(RS_i)^m + K_S^m}\, \frac{K_{L2}^n}{L^n + K_{L2}^n} + V_{L\,min} - \gamma_L\, L.$$

The full model includes LasR and RsaL, assuming separate basal and maximum synthesis rates (V_{min} and V_{max}) for each protein. Here, the Hill function models the dual positive feedback of signal–receptor complex formation on both signal synthase and receptor expression, following a previously proposed notation [28,44]. It considers positive cooperativity through receptor dimerization as above, and the same induction threshold (K_S) for all three proteins, which is consistent with our experimental data (see below). The repression of *lasI* and *rsaL* by RsaL is modelled by the term $K_L^n/(L^n + K_L^n)$, with separate repression constants (K_{L1} and K_{L2}), respectively. This distinction in repression strength is again motivated by our experimental data and is consistent with the asymmetric promoter architecture (even though there is only a single RsaL binding site in the *lasI-rsaL* bidirectional promoter, it is positioned such that disproportionate repression is conceivable) [13]. A Hill coefficient (n) allows for cooperativity in the form of RsaL dimerization [50].

Further, the ODE for extracellular 3OC12-HSL is simplified in both models by assuming a quasi-steady state between intracellular and extracellular signal. Hence, S_e can be expressed through S_i

$$\frac{dS_e}{dt} = \rho_v\, c_{sec}\, (S_i - S_e) - \gamma_{ex}\, S_e = 0$$

$$\Rightarrow S_e = \frac{c_{sec}}{c_{sec} + \gamma_{ex}/\rho_v}\, S_i.$$

Each cellular model is connected to a growing population as follows.

population density, P

$$\frac{dP}{dt} = \mu P\, \frac{(K - P)}{K}$$

and volume fraction, ρ_v

$$\rho_v = N\, \frac{V_{cell}}{V_{tot}} = P\, V_{cell}.$$

Population density P is modelled with a logistic growth equation. P is defined as cell number N (in colony-forming units, CFU) per total culture volume V_{tot} (normalized to 1 l). The volume fraction ρ_v links population growth to the single-cell model through a change in S_e. Strictly speaking, the volume fraction ρ_v is a volume ratio $N(V_{cell})/(V_{tot} - V_{cell})$, which can be readily shown by mass conservation law. However, because V_{cell} is very small compared with V_{tot}, $V_{tot} \cong V_{tot} - V_{cell}$.

Finally, we explicitly model GFP intensities to relate our measurements of *lasI'-gfp*, *lasR'-gfp* and *rsaL'-gfp* reporter expression to the actual protein components in the cell (only *lasI'-gfp* in the reduced model, and all three reporters in the full model).

GFP$_{lasI}$, G_I

$$\frac{dG_I}{dt} = \tau\left((V_{I\,max} - V_{I\,min})\, \frac{(RS_i)^m}{(RS_i)^m + K_S^m}\, \frac{K_{L1}^n}{L^n + K_{L1}^n} + V_{I\,min}\right) - \gamma_G\, G_I,$$

GFP$_{lasR}$, G_R

$$\frac{dG_R}{dt} = \tau\left((V_{R\,max} - V_{R\,min})\, \frac{(RS_i)^m}{(RS_i)^m + K_S^m} + V_{R\,min}\right) - \gamma_G\, G_R$$

and GFP$_{rsaL}$, G_L

$$\frac{dG_L}{dt} = \tau\left((V_{L\,max} - V_{L\,min})\, \frac{(RS_i)^m}{(RS_i)^m + K_S^m}\, \frac{K_{L2}^n}{L^n + K_{L2}^n} + V_{L\,min}\right) - \gamma_G\, G_L.$$

The factor τ relates the rate of GFP synthesis to that of the respective protein. We assume here that promoter activity is proportional to protein concentration. We believe this assumption is appropriate given that QS is a transcriptional regulatory pathway, but of course it neglects possible post-transcriptional effects. The apparent degradation rate of GFP (γ_G) is the same in all equations.

Table 1. Model parameters.

quantity	name	start value[a]	unit	reference	estimated value[c] minimal model	extended model
fittable parameters						
$V_{I\ max}$	maximum LasI synthase expression rate	1.9	μmol (l h)$^{-1}$	[31]	4.2	2.7
$V_{I\ min}$	minimum LasI synthase expression rate	0.022	μmol (l h)$^{-1}$	[31]	0.020	0.017
$V_{R\ max}$	maximum LasR receptor expression rate	1	μmol (l h)$^{-1}$	this study	—	1.3
$V_{R\ min}$	minimum LasR receptor expression rate	0.1	μmol (l h)$^{-1}$	this study	—	0.27
$V_{L\ max}$	maximum RsaL repressor expression rate	1	μmol (l h)$^{-1}$	this study	—	1.0
$V_{L\ min}$	minimum RsaL repressor expression rate	0.1	μmol (l h)$^{-1}$	this study	—	0.0025
K_S	QS induction threshold	0.1	μmol l^{-1}; μmol^2 l^{-2} [b]	[17,18]	0.13	0.11
K_{L1}	repression threshold for *lasI*	1	μmol l^{-1}	this study	—	2.2
K_{L2}	repression threshold for *rsaL*	1	μmol l^{-1}	this study	—	2.8
γ_{ex}	extracellular signal degradation rate	0.0174	h^{-1}	[45]	0.0029	0.0014
c_{sec}	AI transport rate across cell envelope	12	h^{-1}	[16,28]	88	78
A_{syn}	synthesis rate of autoinducer	1.6	h^{-1}	[46,47]	5.5	4.3
γ_I	degradation rate of synthase	0.36	h^{-1}	[31]	1.6	0.78
γ_R	degradation rate of receptor	0.36	h^{-1}	[31]	—	0.42
γ_L	degradation rate of repressor	0.36	h^{-1}	[31]	—	0.093
γ_G	degradation rate of GFP	0.029	h^{-1}	[48]	0.79	0.12
μ	growth rate constant	1.5	h^{-1}	this study	1.3	1.2
K	carrying capacity	3×10^{12}	CFU l^{-1}	this study	2.3×10^{12}	2.4×10^{12}
τ	scaling factor for GFP expression	10 000	Rel. GFP intensity/ (μmol l^{-1})	this study	10 000	10 000
m	Hill coefficient for induction	2	none	[28,49]	2.3	2.2
n	Hill coefficient for repression	2	none	[50]	—	6.8
other parameters						
V_{cell}	volume of a single cell	6×10^{-16}	l	[51,52]	n/a	n/a
V_{tot}	total culture volume	1	l	this study	n/a	n/a
ρ_v	volume fraction of cells	assigned	none	none	n/a	n/a

[a]Start values denote the initial parameter values used in the fitting attempt. In addition to these start values, we defined the initial conditions for the variables in the ODE system at time zero. These were 0.01 μmol l^{-1} for I, R, L and S_i, 100 relative fluorescence intensity units for G_I, G_L, and G_R, and 10^9 CFU l^{-1} for P.

[b]Units are μmol l^{-1} for the minimal model, and μmol^2 l^{-2} for the extended model.

[c]Rounded to two significant figures.

2.4. Model analysis and parameter estimation

The model was built, simulated and analysed with the complex pathway simulator software package (COPASI 4.29) [56,57]. Parameters were estimated with the parameter estimation function (method Levenberg-Marquardt), using the experimental data in figure 1 and the guessed initial parameter values shown in table 1. Parameter fitting was done in iterations, starting with the initial parameter set and then again with the parameter set obtained after the initial step. The fitting algorithm calculates the following objective function, to which each experiment contributes with a weighted sum of squares [57]:

$$E(P) = \sum_{i,j} \omega_j \ (x_{i,j} - y_{i,j} (P))^2,$$

where P is the tested parameter set, $x_{i,j}$ is a point in the dataset, and $y_{i,j}$ is the corresponding simulated value. The indices i and j denote rows and columns in the dataset, corresponding to the measured time points and quantities, respectively. The weight for each data column is given by ω_j. Weights were calculated using the mean squares method.

The Akaike information criterion (AIC) as an estimator of the prediction error was calculated as

$$AIC = n \left(\ln \frac{SSE}{n} \right) + 2k,$$

where n is the number of data points in the dataset, k is the number of parameters fitted plus one and SSE is the least-squares error, i.e. the sum of the objective function in table 2 [58].

A steady-state analysis was conducted with the parameter scan function in Copasi. The GFP$_{lasI}$ level at steady state was determined with cell density as the control variable. To maintain a constant cell density, the growth rate was set to zero, and time courses were run for 1000 h at 1000 different cell density values within a given range.

Table 2. Parameter estimation statistics.

fitted value	data points	minimal model		extended model	
		objective function	RMSE[a]	objective function	RMSE[a]
CFU l^{-1}	15	0.024	0.040	0.014	0.031
[3OC12-HSL]	8	0.80	0.32	0.053	0.082
GFP$_{lasI}$	15	0.080	0.073	0.034	0.048
GFP$_{lasR}$	15	—	—	0.092	0.078
GFP$_{rsaL}$	17	—	—	0.038	0.048
sum	70	0.91	—	0.23	—

[a]RMSE, root mean square error.

Each cell density value was held constant throughout each time course. Two different initial LasI and GFP$_{lasI}$ concentrations were set to separately investigate the off-to-on transition ($I_0 = 0.01$, $G_{I\,0} = 100$) and the on-to-off transition ($I_0 = 1$, $G_{I\,0} = 10\,000$).

2.5. Feedback analysis

To investigate the significance of feedback in the model, we employed the parametrized extended QS model. In addition to S_i, we evaluated effects on the actual circuitry components I, R and L directly, rather than on G_I, G_R and G_L. To essentially eliminate each one of the three feedback loops individually, we set the equilibrium constants in the respective Hill and repression functions to very large values (1×10^6), namely: K_s in the equation for I to eliminate positive feedback on I, K_s in the equation for R to eliminate positive feedback on R, and K_{L1} and K_{L2} in the equations for I and L to eliminate negative feedback on I and L via RsaL. Further, we added a hypothetical QS-controlled protein T to the model to evaluate induction kinetics and steady-state behaviour independent of individual feedback manipulations that alter the kinetics of I, R and L. It follows I induction kinetics but does not include negative influence from RsaL, and the value for K_s remains at 0.11 µmol^2 l^{-2} (table 1).

$$\frac{dT}{dt} = (V_{I\,\max} - V_{I\,\min}) \frac{(RS_i)^m}{(RS_i)^m + K_S^m} + V_{I\,\min} - \gamma_I\, T .$$

3. Results

3.1. Measurement of gene expression and signal production

As a first step, we collected the experimental data required to describe the *las* QS circuit. We focused on species relevant to our mathematical model, and on experimental methods that are feasible and quantitative. We measured the expression of *lasI*, *lasR* and *rsaL* in *P. aeruginosa* via GFP reporter fusions, and we measured the concentration of extracellular 3OC12-HSL by bioassay (figure 2). We used a standard growth medium, buffered Lysogeny broth, that is most commonly used in the field and allows comparison with other studies. We collected time courses across the full range of QS induction dynamics, from basal expression in the off state to maximal expression in the on state.

Consistent with previous studies, we observed a sharp cell density-dependent increase in GFP$_{lasI}$ and GFP$_{rsaL}$ from initially very low, basal levels in the WT strain. The expression of GFP$_{lasR}$ increased concurrently, although basal expression levels were higher. For comparison, the expression of all GFP reporter fusions was much lower in the *lasI* deletion mutant, confirming that their induction is QS-dependent. By contrast to GFP$_{lasI}$ and GFP$_{rsaL}$, GFP$_{lasR}$ showed a modest, partially QS-independent increase throughout growth, the implications of which are discussed below. As expected, the observed concentrations of 3OC12-HSL during culture growth of the WT correlated well with the expression levels of GFP$_{lasI}$.

3.2. Mathematical modelling and parameter estimation

Next, we sought to fit our experimental data to a mechanistic mathematical model of QS. To establish a baseline, we first considered a minimal QS model with single feedback, introduced by Fujimoto & Sawai [28]. This ODE model includes four species, cell density, LasI concentration, extracellular 3OC12-HSL concentration and intracellular 3OC12-HSL concentration. It models positive feedback on *lasI* directly via changes in signal concentration (figure 3 top left; see Methods), with an underlying quasi-steady-state assumption. We amended the model with a GFP equation that directly relates gene expression measured by *lasI'-gfp* fusion to the concentration of LasI in the cell. Hence, three model variables, cell density, extracellular 3OC12-HSL and GFP$_{lasI}$, could be directly fit to experimental data. We asked whether this model is sufficiently complex to describe the experimentally observed induction dynamics. We used the modelling software Copasi [56] to implement the model and estimate parameters using a least-squares method. To guide parameter estimation, start values were taken from our own experimental data when available, or taken from the literature (table 1). In addition to the cell growth data, the minimal model was able to fit the timing of induction well, but failed to accurately capture the subsequent decrease in both 3OC12-HSL and GFP$_{lasI}$ levels (figure 3 and table 2). We reasoned that the negative feedback on *lasI* by RsaL could largely account for the discrepancy.

As a second step, we conducted a parameter estimation with the extended QS model, which incorporates repression of both *lasI* and *rsaL* by RsaL (figure 3 top right). The repression of both genes works by the binding of an RsaL dimer to a conserved sequence element in the *lasI-rsaL* bidirectional promoter [13,14,50]. The extended model also incorporates LasR and its regulation by a second, positive feedback loop, which is supported by our experimental data. We performed a parameter estimation with the extended model as described
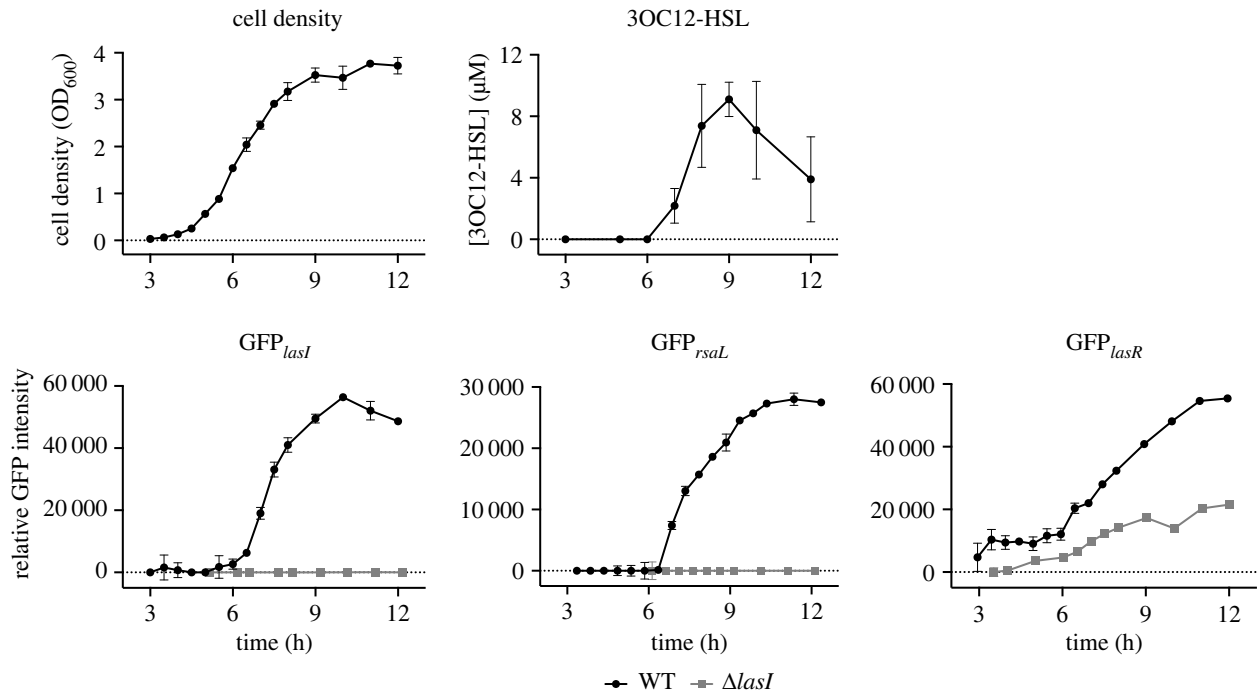
Figure 2. Cell density, signal production, and gene expression in the *P. aeruginosa las* QS circuit. *P. aeruginosa* strains were grown in LB-MOPS batch cultures. Cell density (OD$_{600}$) and 3OC12-HSL production were measured in the WT strain. Gene expression was measured as GFP fluorescence intensity in WT and *lasI* mutant strains containing *lasI'-gfp*, *rsaL'-gfp* or *lasR'-gfp* reporter constructs, respectively. GFP intensity was normalized to cell density. Error bars indicate s.d. (*n* = 3).

above and obtained a greatly improved fit that captured the decline in 3OC12-HSL and GFP$_{lasI}$ levels late in growth. Compared with the minimal model, the extended model showed decreased RMSE values for 3OC12-HSL and GFP$_{lasI}$ (table 2). The RMSE for the newly fit GFP$_{rsaL}$ was equally low, while that for GFP$_{lasR}$ was somewhat higher, possibly indicating additional layers of regulation not captured with our model (see Discussion). Many estimated parameters were remarkably close to the start values used to seed the model (table 1).

To estimate the relative quality of each model, we determined the Akaike information criterion (AIC), which weighs the goodness of fit against the number of parameters used to achieve that fit. The AIC is −116 for the minimal model, and −181 for the extended model (electronic supplementary material, table S1). Because a smaller number indicates higher model quality, we conclude that the extended model performs better, even when considering the larger parameter space.

3.3. Bistability and hysteresis

Having parametrized the extended model, we sought to investigate two important and related emergent properties of the QS network. We asked whether the extended model, as fit to experimental data, can function as a bistable switch with two stable states (on and off), and whether this switch exhibits hysteresis. To answer these questions, we modelled signal synthase expression, GFP$_{lasI}$, at cellular steady state, as a function of different cell densities (figure 4). In support of bistability and hysteresis, we observed two distinct on and off states without a graded transition in between, and we observed sharp transitions at different cell densities, depending on the direction of the change. The cell density range between the low → high and the high → low transition is sizeable, suggesting that hysteresis could significantly improve the stability of the QS response in a fluctuating environment.

Of note, the state switching modelled here is so-called group-level bistability triggered by the accumulation of extracellular signal in a growing population of cells [28]. A concerted group-level response is supported by recent single-cell gene expression data showing unimodal distribution of GFP$_{lasI}$ under culture conditions identical to those used here [17,18].

3.4. The role of positive and negative feedback

Next, we employed the parametrized extended model to analyse the significance of feedback architecture on the QS response. There are two positive feedback loops (LasR-3OC12-HSL activating *lasI* and *lasR*, respectively), and a negative feedback loop (RsaL activated by LasR-3OC12-HSL repressing *lasI* and *rsaL*). We removed one of the respective feedback loops *in silico*, as explained in Methods, and we simulated time courses for the concentrations of the actual QS circuitry components S_e, I, R and L in the modified models (figure 5). To also evaluate these effects on a QS-controlled component that is not itself involved in positive or negative feedback, we added a separate, hypothetical target protein T to the model, and we simulated its behaviour under dynamic and steady-state conditions. In the *P. aeruginosa* LasR regulon, such a target protein candidate would be, for example, the Type VI secretion effector PAAR4, the alkaline protease AprA, or the nucleoside hydrolase Nuh [7,14,59,60].

The omission of positive feedback on I had a large effect. Compared with WT conditions, it delayed the timing of induction, greatly decreased the concentrations of I and S_e and more modestly those of the other components, and resulted in rheostat-like rather than bistable behaviour. Of note, basal expression of I still resulted in the gradual accumulation of S_e to concentrations near the K_s (0.1 μM), such that R, L and T were induced to substantial levels.

By contrast, the omission of positive feedback on R had a much smaller effect. It did not change the magnitude or
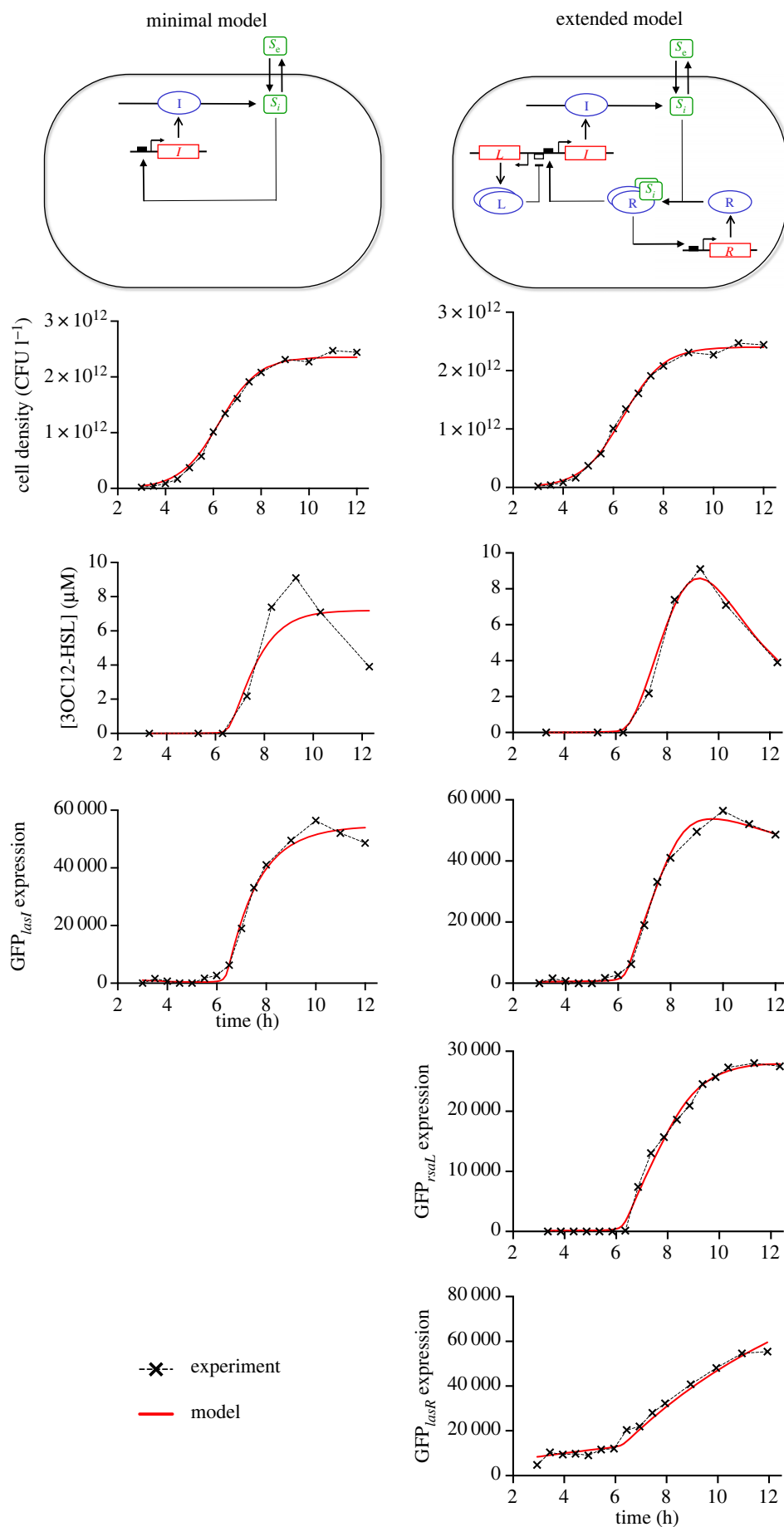
Figure 3. Parametrized models fit to experimental data. The minimal model is shown on the left, and the extended model is shown on the right. Black symbols, experimental data (means from figure 1 with $n = 3$); red line, model fit.
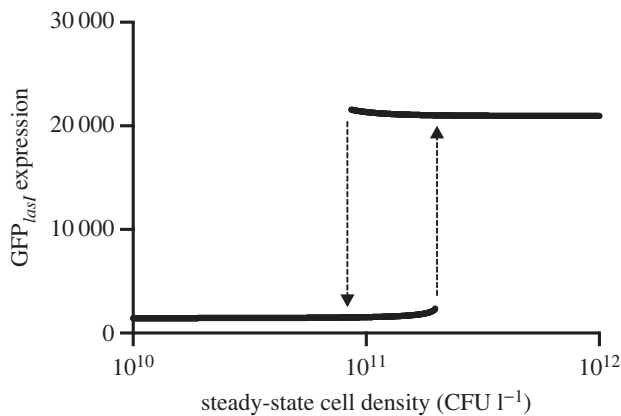
Figure 4. Bistability and hysteresis. Steady-state GFP$_{lasI}$ expression at varying cell densities according to the extended model. This plot represents stable equilibrium conditions, with dG_I/dt = 0 and dP/dt = 0, respectively. Bistability is apparent as two distinct expression states (low or high), lacking a graded transition. Hysteresis is apparent as distinct cell density thresholds (arrows) in the low-to-high and the high-to-low transition.

timing of induction (except for R, of course) and still produced bistable behaviour, albeit with a narrower margin for hysteresis. The observation that positive feedback on I is essential for bistability is consistent with previous theoretical work [30], as is the observation that positive feedback on R enhances hysteresis [26].

The omission of negative feedback on I and L via L had the expected effect on the magnitude of I, L and S_e, but it did not affect the timing of induction, nor bistability in general. The increase in the levels of I, L and S_e is in agreement with experimental data on $lasI$, $rsaL$ and 3OC12-HSL expression in a $P.$ $aeruginosa$ $rsaL$ mutant [14].

4. Discussion

This study brings to bear experimental and mathematical approaches for an integrative understanding of bacterial QS. Experimental and mathematical inquiry has largely co-existed in this field, arguably without much cross-fertilization. Consequently, a systems-level analysis of the functions of native AHL-QS systems in a variety of experimental model species such as *Vibrio fischeri*, *P. aeruginosa*, and *Agrobacterium tumefaciens* remains scarce, and important functional assumptions remain unproven. In this study, we mechanistically modelled the native LasI-LasR (*las*) QS system in *P. aeruginosa*. We fit the model to experimental time series data, and used the parametrized model to investigate feedback architecture and steady-state behaviour, linking network design to function. We found that the parametrized model constitutes a bistable switch with distinct on and off states, as well as hysteretic memory. We also found that positive feedback on signal production is critical in maintaining bistability.

Our chosen modelling approach is one of many [35], but it was guided by the objective to mechanistically describe QS, and to reduce parameter space as much as possible while retaining the ability to explicitly model all experimentally measured variables. Indeed, we found that our extended model is sufficiently complex to accurately describe the experimentally observed QS dynamics. This is remarkable

given that the QS circuitry in *P. aeruginosa* is embedded in global cellular regulation [5,6,61]. However, our focus was exclusively on the *las* system, and there is evidence that this system is more autonomous than the two other, interconnected QS systems, termed *rhl* and *pqs*. The *las* system is considered to be atop the QS hierarchy, and it is influenced less by environmental cues than the *rhl* system [62]. This does not mean that there are no other factors that influence the *las* system [5]. For example, the partially QS-independent increase in *lasR* expression observed experimentally (figure 2) [7,12] is not fully captured by the model. Implementing a clear mechanistic basis for this pattern is not straightforward, as the underlying pathway and level of regulation under the specific culture conditions is not clear. However, it is evident from our feedback analysis that positive feedback on LasR itself is not a critical component of the QS circuitry in *P. aeruginosa*, such that the molecular details of LasR expression are of lesser importance.

Instead, we find that positive signal feedback on *lasI* is required for bistability. This result is consistent with theoretical work by Goryachev *et al.* [29,30]. Goryachev *et al.* also reasoned that a second network element in addition to the classical positive signal feedback is necessary for bistable behaviour. In our network, this second element probably is LasR receptor dimerization. Receptor multimerization is one molecular interaction that contributes to positive cooperativity with a Hill coefficient greater than 1 as estimated in our model. By contrast, experimental and theoretical work by Haseltine and Arnold found that a synthetic QS circuitry with *V. fischeri* components in *E. coli* only exhibits bistability if both *I* and *R* are under positive feedback control [37]. Accordingly, they estimated the Hill coefficient to be 1 in their model (no cooperativity), which neglects *V. fischeri* LuxR receptor dimerization [63], but is consistent with the experimentally determined binding characteristics of LuxR to target DNA [64].

Finally, the omission of negative feedback via RsaL had no major effect on induction dynamics and bistable behaviour. This result indicates that RsaL-mediated repression could mainly function to dampen excessively high signal production, possibly as a cost-saving mechanism, although it is known that RsaL represses many other genes in *P. aeruginosa* besides *lasI* and *rsaL* [14].

It will be interesting to test some of the modelling predictions made here with specific gene deletions, promoter mutations, or target gene-reporter fusions, under dynamic or steady-state growth conditions. It will also be of interest to apply a similar data-based modelling approach to other native QS systems. Individual parameters will differ, and emergent properties may as well, given that a combination of factors (kinetic constants, positive and negative feedback, receptor dimerization and molecular noise) can all affect network behaviour [26,30]. In the case of individual target genes as well as complete QS systems, potential regulatory complexities will need to be considered.

Taken together, our work estimates parameter values and rate constants, and defines design principles and emergent properties of a native QS system. This knowledge can help us quantify the performance of QS in various contexts: in bacterial communities and in association with a host, in the design of synthetic QS circuits with desired functions, and in the development of new therapeutic (quorum-quenching) drugs that target QS in bacterial pathogens.
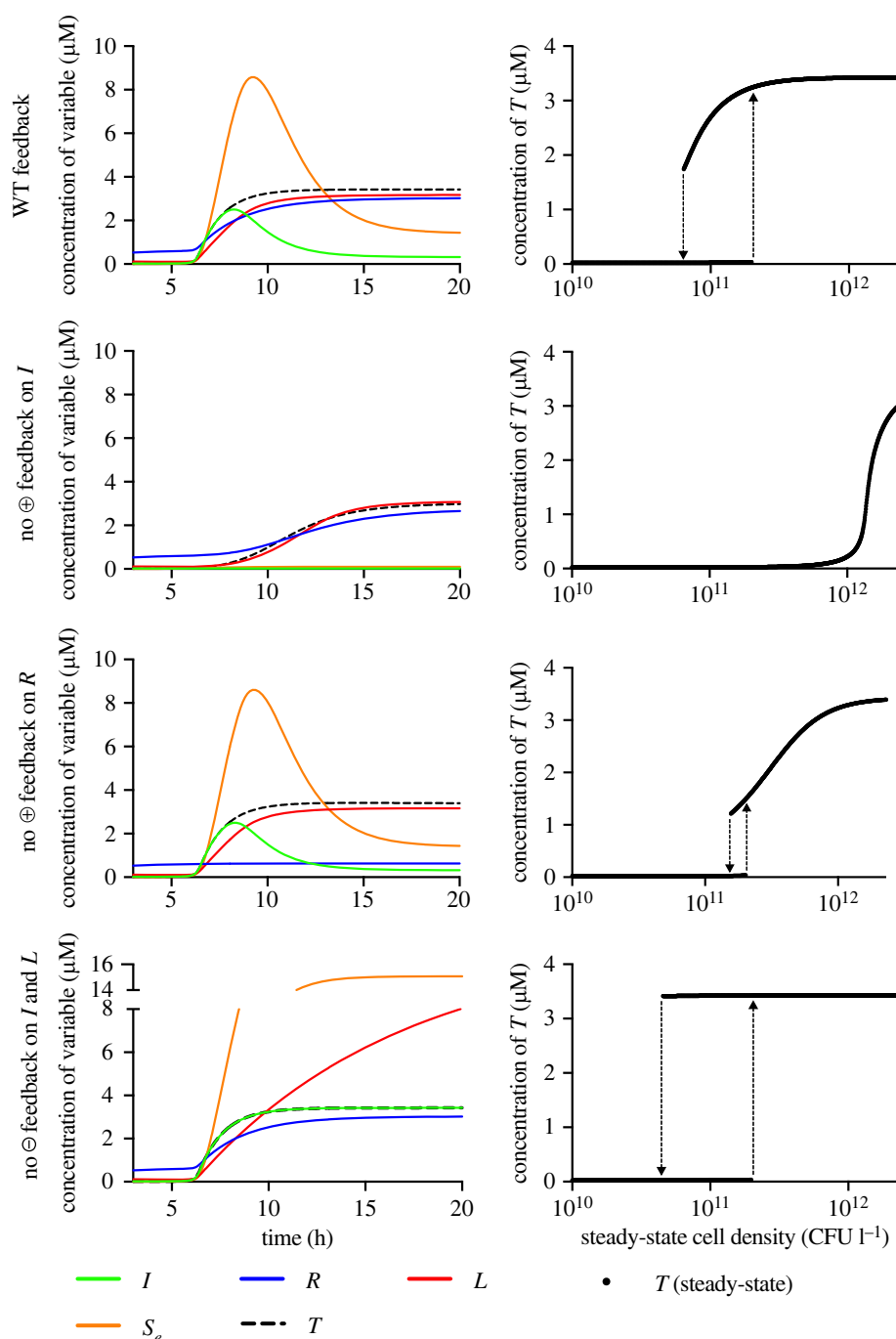
Figure 5. Feedback analysis. The time courses of all QS components, *I* (LasI), *R* (LasR), *L* (RsaL), S_e (extracellular 3OC12-HSL), and a hypothetical target *T*, are shown on the left, and the steady-state behaviour of *T* is shown on the right. The parametrized extended model was simulated with and without positive or negative feedback loops, as indicated by the vertical text on the left. A break was introduced into the y-axis of the bottom left panel in order to keep the scale at the lower concentrations identical to that of the other panels.

References

1. Waters CM, Bassler BL. 2005 Quorum sensing: cell-to-cell communication in bacteria. *Annu. Rev. Cell Dev. Biol.* **21**, 319–346. (doi:10.1146/annurev.cellbio.21.012704.131001)

2. Asfahl KL, Schuster M. 2017 Social interactions in bacterial cell-cell signaling. *FEMS*

Microbiol. Rev. 41, 92–107. (doi:10.1093/femsre/fuw038)

3. Papenfort K, Bassler BL. 2016 Quorum sensing signal-response systems in Gram-negative bacteria. Nat. Rev. Microbiol. 14, 576–588. (doi:10.1038/nrmicro.2016.89)

4. Schuster M, Sexton DJ, Diggle SP, Greenberg EP. 2013 Acyl-homoserine lactone quorum sensing: from evolution to application. Annu. Rev. Microbiol. 67, 43–63. (doi:10.1146/annurev-micro-092412-155635)

5. Schuster M, Greenberg EP. 2006 A network of networks: quorum-sensing gene regulation in Pseudomonas aeruginosa. Int. J. Med. Microbiol. 296, 73–81. (doi:10.1016/j.ijmm.2006.01.036)

6. Williams P, Camara M. 2009 Quorum sensing and environmental adaptation in Pseudomonas aeruginosa: a tale of regulatory networks and multifunctional signal molecules. Curr. Opin Microbiol. 12, 182–191. (doi:10.1016/j.mib.2009.01.005)

7. Schuster M, Lohstroh CP, Ogi T, Greenberg EP. 2003 Identification, timing and signal specificity of Pseudomonas aeruginosa quorum-controlled genes: a transcriptome analysis. J. Bacteriol. 185, 2066–2079. (doi:10.1128/JB.185.7.2066-2079.2003)

8. Wagner VE, Bushnell D, Passador L, Brooks AI, Iglewski BH. 2003 Microarray analysis of Pseudomonas aeruginosa quorum-sensing regulons: effects of growth phase and environment. J. Bacteriol. 185, 2080–2095. (doi:10.1128/JB.185.7.2080-2095.2003)

9. Passos da Silva D, Matwichuk ML, Townsend DO, Reichhardt C, Lamba D, Wozniak DJ, Parsek MR. 2019 The Pseudomonas aeruginosa lectin LecB binds to the exopolysaccharide Psl and stabilizes the biofilm matrix. Nat. Commun. 10, 2183. (doi:10.1038/s41467-019-10201-4)

10. Seed PC, Passador L, Iglewski BH. 1995 Activation of the Pseudomonas aeruginosa lasI gene by LasR and the Pseudomonas autoinducer PAI: an autoinduction regulatory hierarchy. J. Bacteriol. 177, 654–659. (doi:10.1128/jb.177.3.654-659.1995)

11. Fuchs EL, Brutinel ED, Jones AK, Fulcher NB, Urbanowski ML, Yahr TL, Wolfgang MC. 2010 The Pseudomonas aeruginosa Vfr regulator controls global virulence factor expression through cyclic AMP-dependent and -independent mechanisms. J. Bacteriol. 192, 3553–3564. (doi:10.1128/JB.00363-10)

12. Pesci EC, Pearson JP, Seed PC, Iglewski BH. 1997 Regulation of las and rhl quorum sensing in Pseudomonas aeruginosa. J. Bacteriol. 179, 3127–3132. (doi:10.1128/jb.179.10.3127-3132.1997)

13. Rampioni G, Bertani I, Zennaro E, Polticelli F, Venturi V, Leoni L. 2006 The quorum-sensing negative regulator RsaL of Pseudomonas aeruginosa binds to the lasI promoter. J. Bacteriol. 188, 815–819. (doi:10.1128/JB.188.2.815-819.2006)

14. Rampioni G, Schuster M, Greenberg EP, Bertani I, Grasso M, Venturi V, Zennaro E, Leoni L. 2007 RsaL provides quorum sensing homeostasis and functions as a global regulator of gene expression in Pseudomonas aeruginosa. Mol. Microbiol. 66, 1557–1565. (doi:10.1111/j.1365-2958.2007.06029.x)

15. Alcalde-Rico M, Olivares-Pacheco J, Halliday N, Camara M, Martinez JL. 2020 The impaired quorum sensing response of Pseudomonas aeruginosa MexAB-OprM efflux pump overexpressing mutants is not due to non-physiological efflux of 3-oxo-C12-HSL. Environ. Microbiol. 22, 5167–5188. (doi:10.1111/1462-2920.15177)

16. Pearson JP, Van Delden C, Iglewski BH. 1999 Active efflux and diffusion are involved in transport of Pseudomonas aeruginosa cell-to-cell signals. J. Bacteriol. 181, 1203–1210. (doi:10.1128/JB.181.4.1203-1210.1999)

17. Scholz RL, Greenberg EP. 2017 Positive autoregulation of an acyl-homoserine lactone quorum-sensing circuit synchronizes the population response. MBio 8, e01079-17. (doi:10.1128/mBio.01079-17)

18. Smith P, Schuster M. 2022 Antiactivators prevent self-sensing in Pseudomonas aeruginosa quorum sensing. Proc. Natl. Acad. Sci. USA 119, e2201242119. (doi:10.1073/pnas.2201242119)

19. Darch SE, West SA, Winzer K, Diggle SP. 2012 Density-dependent fitness benefits in quorum-sensing bacterial populations. Proc. Natl. Acad. Sci. USA 109, 8259–8263. (doi:10.1073/pnas.1118131109)

20. Fuqua WC, Winans SC, Greenberg EP. 1994 Quorum sensing in bacteria: the LuxR-LuxI family of cell density-responsive transcriptional regulators. J. Bacteriol. 176, 269–275. (doi:10.1128/jb.176.2.269-275.1994)

21. Pai A, Tanouchi Y, You L. 2012 Optimality and robustness in quorum sensing (QS)-mediated regulation of a costly public good enzyme. Proc. Natl. Acad. Sci. USA 109, 19 810–19 815. (doi:10.1073/pnas.1211072109)

22. Anetzberger C, Pirch T, Jung K. 2009 Heterogeneity in quorum sensing-regulated bioluminescence of Vibrio harveyi. Mol. Microbiol. 73, 267–277. (doi:10.1111/j.1365-2958.2009.06768.x)

23. Grote J et al. 2014 Evidence of autoinducer-dependent and -independent heterogeneous gene expression in Sinorhizobium fredii NGR234. Appl. Environ. Microbiol. 80, 5572–5582. (doi:10.1128/AEM.01689-14)

24. Perez PD, Hagen SJ. 2010 Heterogeneous response to a quorum-sensing signal in the luminescence of individual Vibrio fischeri. PLoS ONE 5, e15473. (doi:10.1371/journal.pone.0015473)

25. Rattray JB, Thomas SA, Wang Y, Molotkova E, Gurney J, Varga JJ, Brown SP. 2022 Bacterial quorum sensing allows graded and bimodal cellular responses to variations in population density. mBio 13, e0074522. (doi:10.1128/mbio.00745-22)

26. Williams JW, Cui X, Levchenko A, Stevens AM. 2008 Robust and sensitive control of a quorum-sensing circuit by two interlocked feedback loops. Mol. Syst. Biol. 4, 234. (doi:10.1038/msb.2008.70)

27. Dockery JD, Keener JP. 2001 A mathematical model for quorum sensing in Pseudomonas aeruginosa. Bull. Math. Biol. 63, 95–116. (doi:10.1006/bulm.2000.0205)

28. Fujimoto K, Sawai S. 2013 A design principle of group-level decision making in cell populations. PLoS Comput. Biol. 9, e1003110. (doi:10.1371/journal.pcbi.1003110)

29. Goryachev AB. 2011 Understanding bacterial cell-cell communication with computational modeling. Chem. Rev. 111, 238–250. (doi:10.1021/cr100286z)

30. Goryachev AB, Toh DJ, Lee T. 2006 Systems analysis of a quorum sensing network: design constraints imposed by the functional requirements, network topology and kinetic constants. Biosystems 83, 178–187. (doi:10.1016/j.biosystems.2005.04.006)

31. Goryachev AB, Toh DJ, Wee KB, Lee T, Zhang HB, Zhang LH. 2005 Transition to quorum sensing in an Agrobacterium population: a stochastic model. PLoS Comput. Biol. 1, e37. (doi:10.1371/journal.pcbi.0010037)

32. Kuttler C, Hense BA. 2008 Interplay of two quorum sensing regulation systems of Vibrio fischeri. J. Theor. Biol. 251, 167–180. (doi:10.1016/j.jtbi.2007.11.015)

33. Muller J, Kuttler C, Hense BA. 2008 Sensitivity of the quorum sensing system is achieved by low pass filtering. Biosystems 92, 76–81. (doi:10.1016/j.biosystems.2007.12.004)

34. Pai A, You L. 2009 Optimal tuning of bacterial sensing potential. Mol. Syst. Biol. 5, 286. (doi:10.1038/msb.2009.43)

35. Perez-Velazquez J, Golgeli M, Garcia-Contreras R. 2016 Mathematical modelling of bacterial quorum sensing: a review. Bull. Math. Biol. 78, 1585–1639. (doi:10.1007/s11538-016-0160-6)

36. Ward JP, King JR, Koerber AJ, Croft JM, Sockett RE, Williams P. 2004 Cell-signalling repression in bacterial quorum sensing. Math. Med. Biol. 21, 169–204. (doi:10.1093/imammb/21.3.169)

37. Haseltine EL, Arnold FH. 2008 Implications of rewiring bacterial quorum sensing. Appl. Environ. Microbiol. 74, 437–445. (doi:10.1128/AEM.01688-07)

38. Holloway BW. 1955 Genetic recombination in Pseudomonas aeruginosa. J. Gen. Microbiol. 13, 572–581.

39. Miller WG, Leveau JH, Lindow SE. 2000 Improved gfp and inaZ broad-host-range promoter-probe vectors. Mol. Plant Microbe Interact. 13, 1243–1250. (doi:10.1094/MPMI.2000.13.11.1243)

40. Cormack BP, Valdivia RH, Falkow S. 1996 FACS-optimized mutants of the green fluorescent protein (GFP). Gene 173, 33–38. (doi:10.1016/0378-1119(95)00685-0)

41. Chuanchuen R, Narasaki T, Schweizer HP. 2002 Benchtop and microcentrifuge preparation of Pseudomonas aeruginosa competent cells. Biotechniques 33, 760–763. (doi:10.2144/02334bm08)

42. Pearson JP, Gray KM, Passador L, Tucker KD, Eberhard A, Iglewski BH, Greenberg EP. 1994 Structure of the autoinducer required for expression of Pseudomonas aeruginosa virulence genes. Proc. Natl. Acad. Sci. USA 91, 197–201. (doi:10.1073/pnas.91.1.197)

43. Pearson JP, Passador L, Iglewski BH, Greenberg EP. 1995 A second N-acylhomoserine lactone signal produced by Pseudomonas aeruginosa. Proc. Natl.

Acad. Sci. USA **92**, 1490–1494. (doi:10.1073/pnas. 92.5.1490)

44. Rai N, Anand R, Ramkumar K, Sreenivasan V, Dabholkar S, Venkatesh KV, Thattai M. 2012 Prediction by promoter logic in bacterial quorum sensing. *PLoS Comput. Biol.* **8**, e1002361. (doi:10. 1371/journal.pcbi.1002361)

45. Kaufmann GF *et al.* 2005 Revisiting quorum sensing: discovery of additional chemical and biological functions for 3-oxo-N-acylhomoserine lactones. *Proc. Natl Acad. Sci. USA* **102**, 309–314. (doi:10.1073/pnas.0408639102)

46. More MI, Finger LD, Stryker JL, Fuqua C, Eberhard A, Winans SC. 1996 Enzymatic synthesis of a quorum-sensing autoinducer through use of defined substrates. *Science* **272**, 1655–1658. (doi:10.1126/ science.272.5268.1655)

47. Schaefer AL, Val DL, Hanzelka BL, Cronan Jr JE, Greenberg EP. 1996 Generation of cell-to-cell signals in quorum sensing: acyl homoserine lactone synthase activity of a purified Vibrio fischeri LuxI protein. *Proc. Natl Acad. Sci. USA* **93**, 9505–9509. (doi:10.1073/pnas.93.18.9505)

48. Andersen JB, Sternberg C, Poulsen LK, Bjorn SP, Givskov M, Molin S. 1998 New unstable variants of green fluorescent protein for studies of transient gene expression in bacteria. *Appl. Environ. Microbiol.* **64**, 2240–2246. (doi:10.1128/AEM.64.6.2240-2246.1998)

49. Bottomley MJ, Muraglia E, Bazzo R, Carfi A. 2007 Molecular insights into quorum sensing in the human pathogen *Pseudomonas aeruginosa* from the structure of the virulence regulator LasR bound to its autoinducer. *J. Biol. Chem.* **282**, 13 592–13 600. (doi:10.1074/jbc.M700556200)

50. Kang H *et al.* 2017 Crystal structure of *Pseudomonas aeruginosa* RsaL bound to promoter DNA reaffirms its role as a global regulator involved in quorum-sensing. *Nucleic Acids Res.* **45**, 699–710. (doi:10. 1093/nar/gkw954)

51. Lynch M, Marinov GK. 2015 The bioenergetic costs of a gene. *Proc. Natl Acad. Sci. USA* **112**, 15 690–15 695. (doi:10.1073/pnas.1514974112)

52. Milo R, Jorgensen P, Moran U, Weber G, Springer M. 2010 BioNumbers—the database of key numbers in molecular and cell biology. *Nucleic Acids Res.* **38**, D750–D753. (doi:10.1093/nar/gkp889)

53. Kiratisin P, Tucker KD, Passador L. 2002 LasR, a transcriptional activator of *Pseudomonas aeruginosa* virulence genes, functions as a multimer. *J. Bacteriol.* **184**, 4912–4919. (doi:10.1128/JB.184. 17.4912-4919.2002)

54. Schuster M, Urbanowski ML, Greenberg EP. 2004 Promoter specificity in *Pseudomonas aeruginosa* quorum sensing revealed by DNA binding of purified LasR. *Proc. Natl. Acad. Sci. USA.* **101**, 15 833–15 839. (doi:10.1073/pnas.0407229101)

55. Klumpp S, Hwa T. 2014 Bacterial growth: global effects on gene expression, growth feedback and proteome partition. *Curr. Opin Biotechnol.* **28**, 96–102. (doi:10.1016/j.copbio.2014. 01.001)

56. Hoops S *et al.* 2006 COPASI–a COmplex PAthway SImulator. *Bioinformatics* **22**, 3067–3074. (doi:10. 1093/bioinformatics/btl485)

57. Mendes P, Hoops S, Sahle S, Gauges R, Dada J, Kummer U. 2009 Computational modeling of biochemical networks using COPASI. *Methods Mol. Biol.* **500**, 17–59. (doi:10.1007/978-1-59745-525-1_2)

58. Cavanaugh JE, Neath AA. 2019 The Akaike information criterion: Background, derivation, properties, application, interpretation, and refinements. *Wires Comp. Stat.* **11**, e1460. (doi:10. 1002/wics.1460)

59. Gilbert KB, Kim TH, Gupta R, Greenberg EP, Schuster M. 2009 Global position analysis of the *Pseudomonas aeruginosa* quorum-sensing transcription factor LasR. *Mol. Microbiol.* **73**, 1072–1085. (doi:10.1111/j.1365-2958.2009.06832.x)

60. Schuster M, Greenberg EP. 2007 Early activation of quorum sensing in *Pseudomonas aeruginosa* reveals the architecture of a complex regulon. *BMC Genomics* **8**, 287. (doi:10.1186/1471-2164-8-287)

61. Lee J, Zhang L. 2015 The hierarchy quorum sensing network in *Pseudomonas aeruginosa*. *Protein Cell* **6**, 26–41. (doi:10.1007/s13238-014-0100-x)

62. Mellbye B, Schuster M. 2014 Physiological framework for the regulation of quorum sensing-dependent public goods in *Pseudomonas aeruginosa*. *J. Bacteriol.* **196**, 1155–1164. (doi:10. 1128/JB.01223-13)

63. Choi SH, Greenberg EP. 1992 Genetic evidence for multimerization of LuxR, the transcriptional activator of *Vibrio fischeri* luminescence. *Mol. Mar. Biol. Biotech.* **1**, 408–413.

64. Urbanowski ML, Lostroh CP, Greenberg EP. 2004 Reversible acyl-homoserine lactone binding to purified *Vibrio fischeri* LuxR protein. *J. Bacteriol.* **186**, 631–637. (doi:10.1128/JB.186.3.631-637.2004)

65. Schuster M, Li C, Smith P, Kuttler C. 2023 Parameters, architecture, and emergent properties of the *Pseudomonas aeruginosa* LasI/LasR quorum-sensing circuit. Figshare. (doi:10.6084/m9.figshare.c.6451363)